SPACE
TELESCOPE
SCIENCE
INSTITUTE

Instrument Science Report STIS 2009-02

STIS CCD Performance after SM4:
Read Noise, Dark Current, Hot Pixel Annealing, CTE, Gain, and Spectroscopic Sensitivity

Paul Goudfrooij, Michael A. Wolfe, Ralph C. Bohlin, Charles R. Proffitt, & Daniel J. Lennon

October 30, 2009

ABSTRACT

We describe the overall performance of the STIS CCD after HST Servicing Mission #4 and the associated updates to calibration reference files. Most aspects of CCD performance are found to be fairly consistent with extrapolations of the trends seen prior to the failure of STIS in August 2004. The CCD gain value for the CCDGAIN = 4 setting has been redetermined using net count ratios of standard star spectra taken in the CCDGAIN = 1 and CCDGAIN = 4 settings, resulting in a gain value of $4.016 \pm 0.003\ e^-$/DN, which is 0.5% lower than the value used for the calibration of archival STIS CCD data taken before August 2004. Finally, we identify two independent indications of a temperature dependence of the Charge Transfer Efficiency (CTE). However, more calibration data are needed to verify the significance of this effect and, if verified, to calibrate it as a function of CCD housing temperature (as a proxy for CCD chip temperature). This option will be reassessed later during the Cycle 17 calibration program.

1   Introduction

As the STIS instrument has been dormant for over 4.5 years before a successful repair during the HST Servicing Mission #4 (SM4), its performance and the applicability of the calibrations implemented during the "STIS Closeout Project" after the failure of STIS in August 2004 (Goudfrooij et al. 2006a; we happily acknowledge the now inappropriate name of this past project) need to be verified. This report describes the analysis of the performance of the STIS CCD as measured during the Servicing Mission Orbital Verification (SMOV) period after SM4, hereafter referred to as SMOV4.

2 CCD Read Noise and Structure of Bias Frames

2.1 Evolution of Read Noise

Figure 1 shows the history of read noise (hereafter RN) values for the STIS CCD as measured from pairs of unbinned BIAS frames in the CCDGAIN = 1 and CCDGAIN = 4 settings, using the nominal readout amplifier D, which is located at the top right of the CCD. The measurement involves the subtraction of one bias frame from another (taken in the same observing sequence) in order to eliminate the effect of the varying 2-D structure in the bias signal across the CCD from the noise measurements. The measurements are done in numerous subareas within the bias frame to allow the identification of any systematic uncertainty of the RN values.
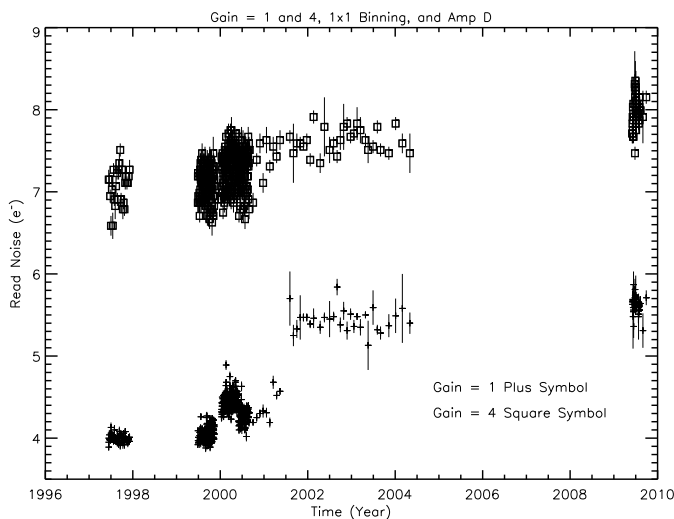

Figure 1: The evolution of the read noise for the two supported CCD gain settings. See discussion in §2.1.

While STIS was operating on its side-1 electronics, the effective RN of the CCDGAIN = 1 and CCDGAIN = 4 modes started out at ~ 4.0 e$^-$ and ~ 7.1 e$^-$, respectively. After SM3A (Dec 1999), the RN of the CCDGAIN = 1 mode increased to an average of ~ 4.4 e$^-$ while the RN of the CCDGAIN = 4 mode only increased very slightly[1]. After the switch to the side-2 electronics in July 2001, an extra component of electronic pick-up noise caused RN values to increase to ~ 5.4 e$^-$ and ~ 7.7 e$^-$ for CCDGAIN = 1 and 4, respectively. As Fig. 1 shows, the post-SM4 measurements to date show average RN values that are slightly higher than the pre-SM4 values, namely 5.6 e$^-$ and 8.0 e$^-$ for CCDGAIN = 1 and 4, respectively. The STIS team continues to monitor CCD RN values on a monthly basis.

2.2 Evolution of Structure of Bias Frames

The STIS CCD features a structure along columns (i.e., along the parallel clocking direction), which is commonly referred to as "spurious charge" (Goudfrooij & Walsh 1997). This structure is due to a small amount of charge "leakage" during pre-flush and readout, and effectively causes a position-dependent background level (even though it is subtracted out during the BIASCORR step within the STIS calibration pipeline CALSTIS). The amplitude and slope of this structure have been found to increase with on-orbit time. This is depicted in Fig. 2, where the spurious charge level is plotted as a function of time for all weekly superbias reference files

---

[1]The root cause of the read noise increase after SM3A was never uncovered by an HST Anomaly Review Board

created as of October 16, 2009, for two locations on the chip (the central row and row 900, where the so-called E1 and E2 pseudo-apertures[2] are located). The cause of this phenomenon (which is also seen for dark frames, see § 3.2 below) is thought to be the accumulation of radiation damage of the CCD: Each hot pixel leaves behind not only a charge tail due to Charge Transfer Efficiency (CTE) loss (cf. § 5 below), but also a plateau of dribbled electrons from chip flaws into each charge packet. The ramp vs. row number results from adding together many such step functions at random locations. The slope thus increases along with the number and intensity of hot pixels.

For the nominal CCDGAIN = 1 setting, the post-SM4 superbiases show a mean level and slope of the spurious charge ramp that are approximately 60% larger than in the pre-failure era. As the spurious charge level is relevant to the correction for CTE loss in CALSTIS (especially for faint targets; cf. § 5 below), we created a new STIS CCD Parameter Table (header keyword CCDTAB)[3] with current values for the spurious charge level at the center of the CCD. Given the increasing slope of the spurious charge along columns, the STIS team is currently preparing a more comprehensive update of the calibration pipeline which will allow a more precise CTE correction across the whole CCD. This will be reported on separately.
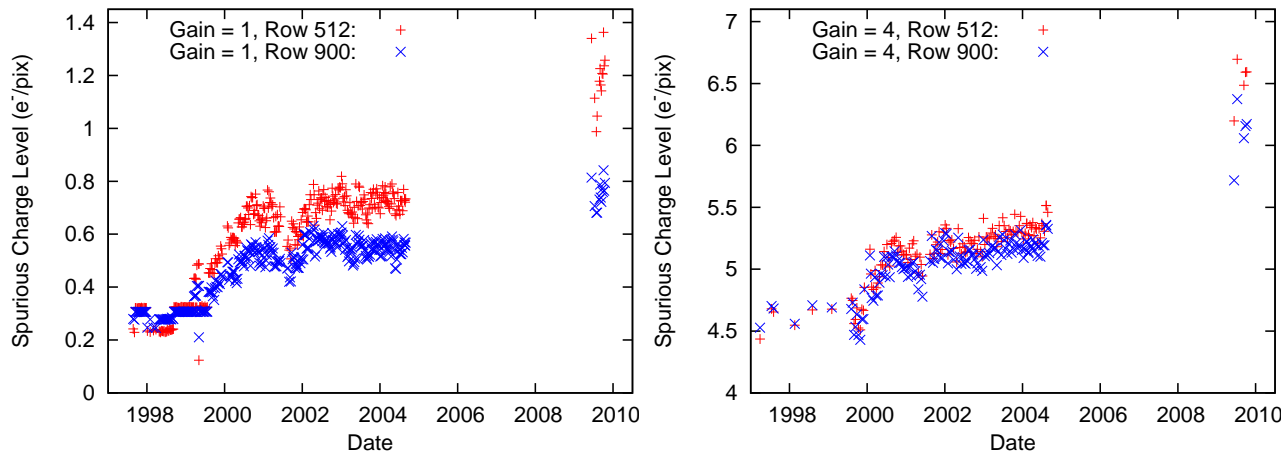

Figure 2: The evolution of the spurious charge level for the two supported CCD gain settings and two locations on the chip (see legend in top left of each panel). Error bars are similar to the spread among the data points at a given time. See discussion in § 2.2.

3 CCD Dark Current and Hot Pixel Annealing

One of the effects of accumulative ionizing radiation damage to CCDs in the HST environment is a continuous increase of dark current with time. This is mainly due to "localized" damage defects caused by fast electrons which in turn are caused by high-energy photon interactions. The affected pixels are generally called "hot" or "warm" pixels, and they can encompass a wide range of signal levels. Periodic thermal annealing of the CCD changes many of these pixels back to their original (lower) dark current state. STIS operations perform anneals on a roughly monthly time scale by letting the CCD warm up to the ambient temperature (of about +5 °C) for several hours. This procedure does decrease the number of "hot" pixels, but cannot prevent a general increase of both the number of hot pixels and the overall median dark current with time. More details on the annealing

---

[2]See Chapter 4.2.3 of the STIS Instrument Handbook

[3]See final paragraph of § 5.2.1 for details about this new version of the CCDTAB

procedure and its effect on the increasing numbers of hot pixels on the STIS CCD prior to SM4 are available in Hayes et al. (1998) and Wolfe et al. (2009). In this report, we show and discuss the main results from the CCD anneal executions that took place during the first four months after SM4, supplemented by information on the evolution of the median dark current with time as derived from the dark reference files that are produced on a weekly basis (see, e.g., Chapter 4.1.3 of the STIS Data Handbook).

3.1   CCD Anneals

Figure 3 shows the evolution of the number of hot pixels in post-anneal superdark frames for five count-rate cuts. After a steady and approximately linear increase in the number of hot pixels from STIS installation in March 1997 to the failure of the side-1 electronics on May 16, 2001, the number of hot pixels briefly decreased after the switch to the side-2 electronics. This was likely due to a lower CCD temperature after the switch; the side-2 setup features a constant current through the CCD cooler which is higher than the average current used on side 1. The hot pixel rate increased again from mid-2001 until the STIS failure in August 2004, albeit at a somewhat lower rate than it did on side 1. As Figure 3 shows, the post-SMOV data reveal post-anneal hot pixel rates that are slightly higher than those predicted from a linear extrapolation of the pre-SM4 side-2 data. The current fraction of CCD pixels with dark rates ≥ 0.1 e$^-$/s is $\sim 3.4\%$, making proper dithering of STIS CCD observations now even more important than before the failure in August 2004.
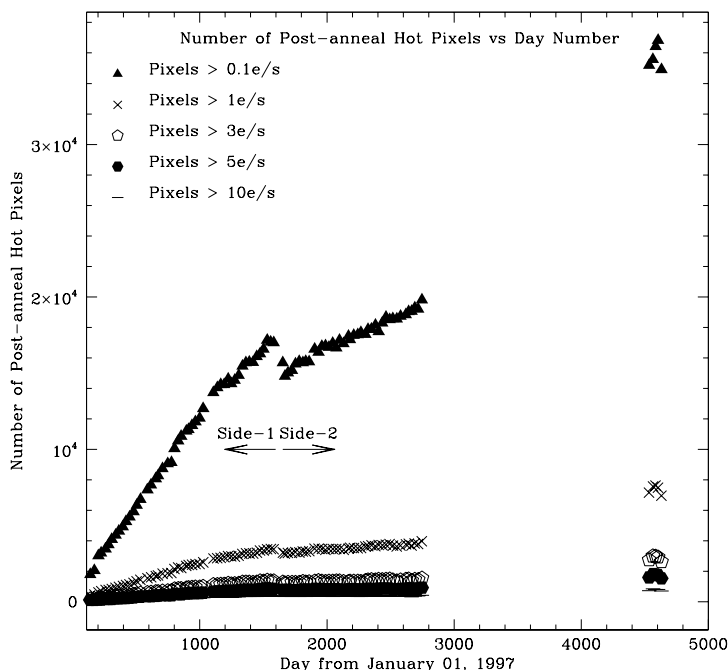

Figure 3: Total number of post-anneal hot pixels at different count-rate cuts as a function of on-orbit time. The date when STIS switched to its Side-2 electronics is indicated by arrows. The growth rate of hot pixels decreased after the switch to Side 2 due to the CCD running at cooler temperatures than on Side 1, but remained roughly linear up to the demise of STIS in August 2004. The few months' worth of post-SM4 data show somewhat higher numbers than those expected from an extrapolation of the pre-SM4 side-2 values.

Percentages of hot pixels remaining after CCD anneals are depicted in Fig. 4, both in terms of percentages of *all* hot pixels remaining after an anneal (left panel) and as percentages of *new* hot pixels accumulated during
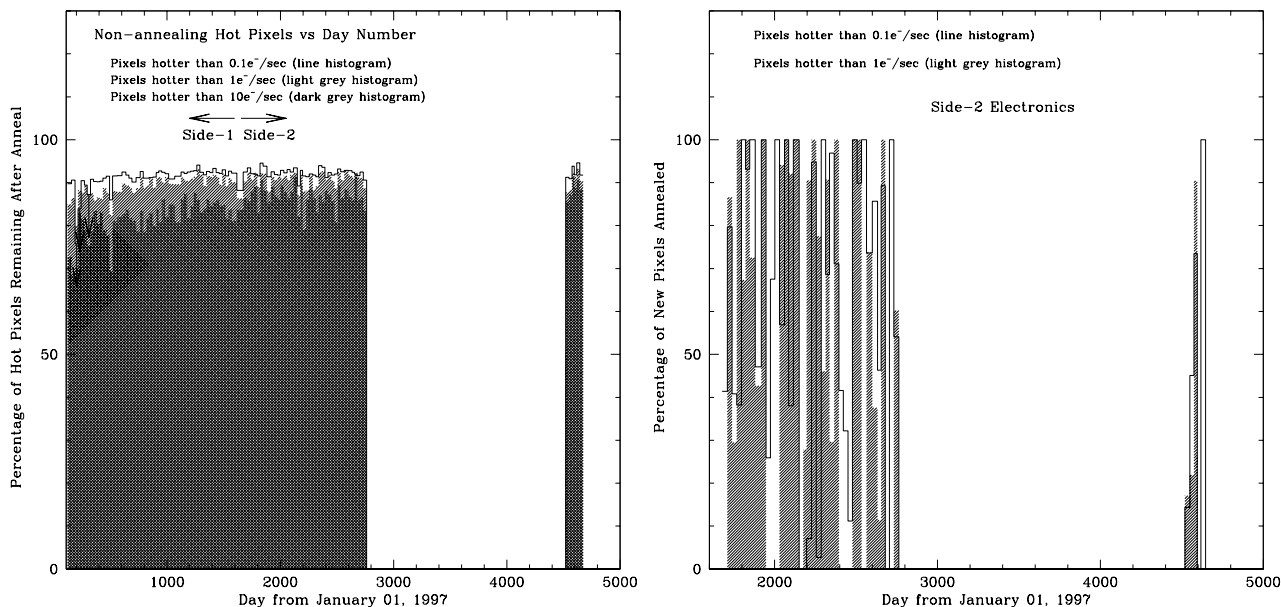
Figure 4: *Left Panel:* Histogram of the percentage of all hot pixels that persist after each anneal versus on-orbit time. Different shading greyscales represent different count-rate cuts as shown in the legend. The date when STIS switched to its Side-2 electronics is indicated by arrows towards the left and right. Downward arrows represent upper limits for some of the early data points (those anneals used 3 dark exposures instead of 5). *Right Panel:* Percentage of "new" hot pixels annealed in a given month versus on-orbit time for two count-rate cuts as shown in the legend.

an anneal period that the anneal eliminated (right panel). The "anneal rates" in the post-SM4 era remained consistent with those seen during pre-SM4 side-2 operations. STIS CCD annealing reports are always available on-line through the STIS web site[4] through the "Monitoring" link on the left-hand side.

3.2 CCD Dark Current and its Evolution

The long term trend of the median dark current level of the STIS CCD is shown in Fig. 5. Recall that the CCD temperature was stabilized at $-83\,°C$ from March 1997 until the failure of the side-1 electronics. After the switch to the side-2 electronics in July 2001, the CCD temperature could not be stabilized anymore so that thermal fluctuations impacted the dark current since then. These fluctuations are being parameterized in terms of the CCD housing temperature which are being recorded in the science data headers. The side-2 dark current values in Fig. 5 are normalized to a CCD Housing Temperature of $18\,°C$ using the scaling relation determined by Brown (2001). Dark current values in Fig. 5 are shown for three areas on the CCD: *(i)* The full CCD (open black circles), *(ii)* the central 200×200 pixels area (red pluses), and *(iii)* an area of 200×200 pixels near the top center of the CCD (open blue squares). Note that the dark current level is increasing more slowly for the top of the CCD than it is for the center (or the full CCD), i.e., there is a slope in the dark current along CCD columns which is increasing with time, just like the spurious charge in CCD Bias frames as discussed in § 2.2 above. To put the measured SMOV4 values of the dark current in perspective, we also depict two possible extrapolations of the pre-SM4 values in Fig. 5. The solid lines show the extrapolation of a linear fit to the last year of pre-SM4
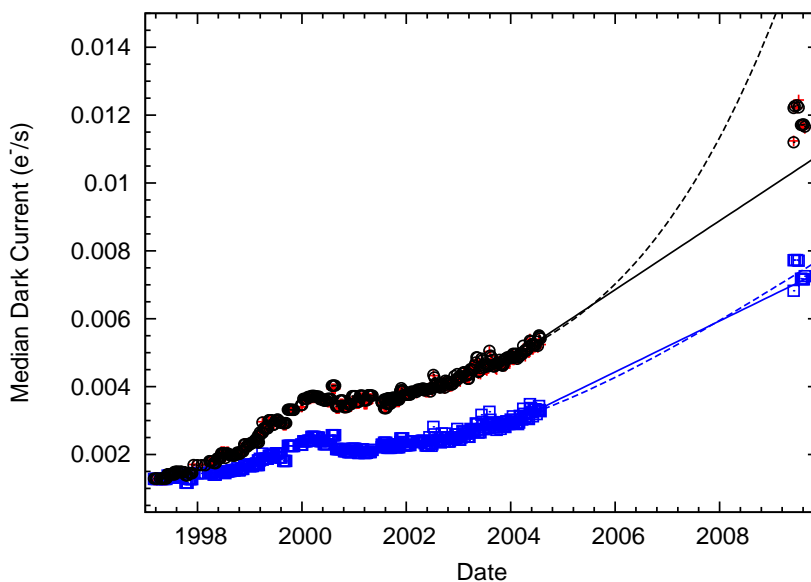
---

[4]http://www.stsci.edu/hst/stis

Figure 5: The time evolution of the median dark current of the STIS CCD. Open black circles represent values for the whole CCD, red pluses represent values for an area of 200×200 pixels at the center of the CCD, and open blue squares represent values for an area of 200×200 pixels near the top center of the CCD. The solid and dashed line depict extrapolations of linear and cubic fits to the $2002-2004$ data with the corresponding symbol colors, respectively. Side-2 data (after epoch 2001.5) have been normalized to a CCD housing temperature of 18 °C. See discussion in §3.2.

dark values, while the dashed lines do so for a cubic fit to all pre-SM4 side-2 values. Both extrapolations fit the SMOV4 data near the top of the CCD equally well, while the SMOV4 data for the full (or the center of the) CCD fall in between the two extrapolations. The STIS team continues to monitor the dark current carefully to make sure calibrations stay up to date.

4 CCD Gain Values

The nominal gain setting for the STIS CCD is CCDGAIN = 1. The gain value for this setting was determined during ground calibration by means of the "mean-variance method", measuring the slope of variance vs. mean intensity level for a large set of flatfield exposures. This resulted in a gain value of 1.000 ± 0.008 e⁻/DN. As the tungsten lamp on-board STIS is too bright to allow such a measurement, the STIS team has monitored this gain setting annually by means of a less-accurate method (see Goudfrooij et al. 1997; Dashevsky et al. 2000; Diaz-Miller et al. 2001; Proffitt et al. 2003; Dressel et al. 2004). The gain value for CCDGAIN = 1 has always stayed consistent with the ground calibration measurement. For the CCDGAIN = 4 setting, the ground calibration measurement was not done accurately. The most accurate on-orbit measurements utilized net count ratios of spectra of flux standard stars in the two supported CCDGAIN settings. The last such measurement was done in 2000, before accurate CTE corrections were available (Smith et al. 2000). We re-performed this measurement using CTE-corrected data from several visits of the CCD spectroscopic sensitivity calibration programs (described further in §6.2 below). Specifically, we used nine ratio spectra: *(i)* eight G430L spectra of AGK+81D266 taken in CCDGAIN = 4 divided by an average G430L spectrum taken in CCDGAIN = 1, and

(ii) one ratio spectrum composed of average G230LB spectra of G191B2B taken in the CCDGAIN = 4 and 1 modes. This measurement resulted in a new value of 4.016 ± 0.003 e$^-$/DN. Fig. 6 shows the residuals of the ratio spectra after taking the new gain=4/gain=1 ratio into account.
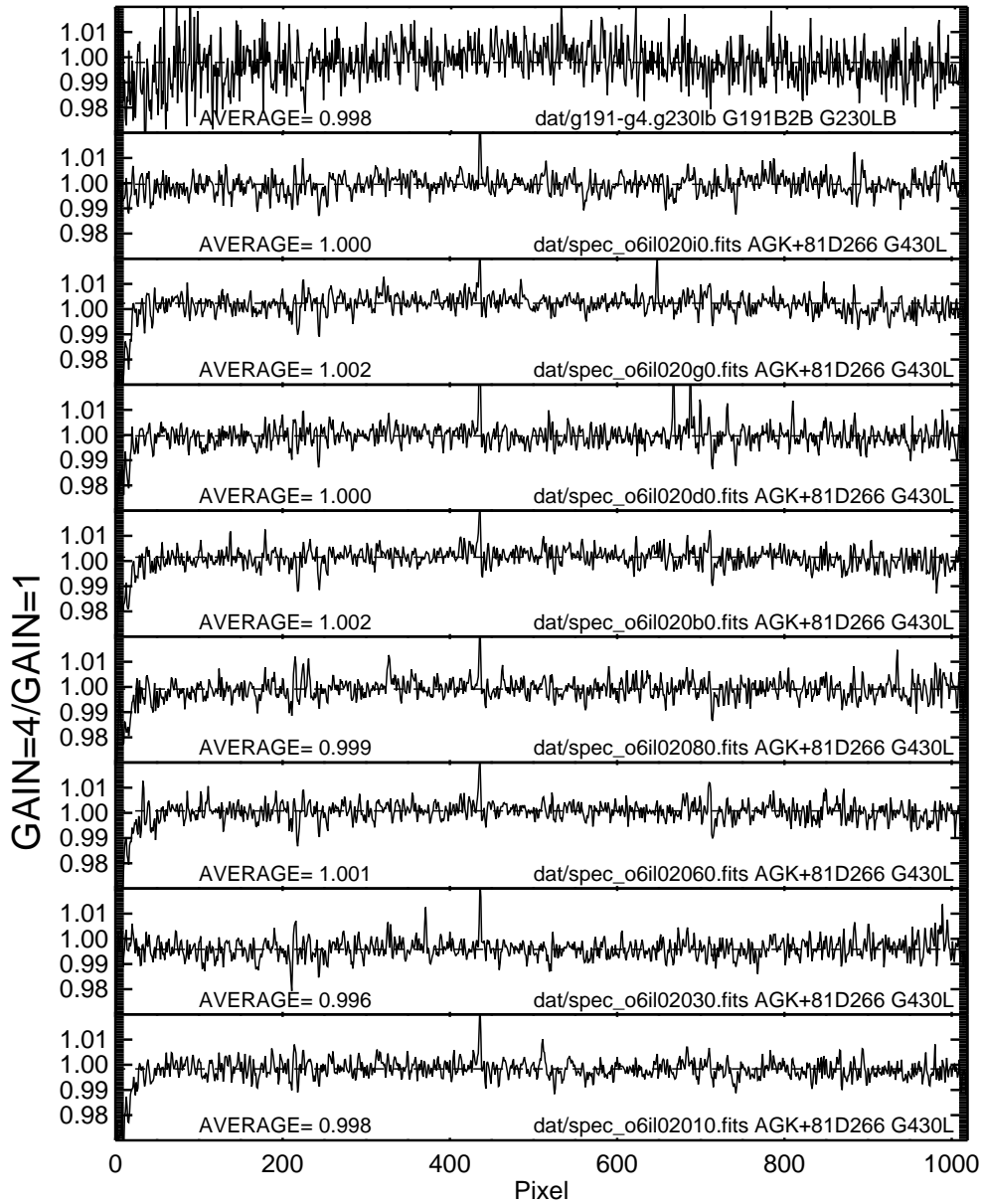

Figure 6: Normalized net count ratio of 9 pairs of flux standard star spectra taken in CCDGAIN = 1 and CCDGAIN = 4 modes. The normalization factor yielding the smallest residuals among the pairs of spectra is 4.016, which is adopted as the gain=4/gain=1 gain ratio.

5   Charge Transfer Efficiency

A well-known effect of radiation damage for CCDs in HST instruments is a continuous decrease of CTE due to an increasing population of charge traps in the silicon of CCDs, which are caused by nuclear reactions (due to impacts by neutrons or high-energy protons). In practice one often uses the term Charge Transfer *Inefficiency* (CTI $\equiv 1-$CTE), which we do in the remainder of this section. The main observational effect of CTI is that a star whose induced charge has to traverse many pixels before being read out appears to be fainter than the same star observed near the read-out amplifier. Several aspects of on-orbit characterizations of the CTI of the STIS CCD were reported by Goudfrooij & Bohlin (2006), Goudfrooij et al. (2006b), and references therein.

Here we report on the results of two CTI tests executed during SMOV4 and compare with results of the same tests executed periodically during STIS's "first life" (1997-2004).

5.1   Extended Pixel Edge Response Test

The "Extended Pixel Edge Response" (EPER) test (Janesick et al. 1991) is a popular technique for measuring CTI since it typically does not require any specialized equipment. The EPER test measures the charge in the overscan region of the CCD in a uniformly illuminated exposure after subtraction of the overscan bias level. This excess charge is due to the release of deferred charge (which is due to imperfect CTE) after clocking a whole column or row of the sensitive part of the CCD, and appears as an exponential tail. The estimated CTI from EPER measurements is

$$\text{CTI}_{\text{EPER}} = \frac{S_D}{S_{LC}\, N_P} \tag{1}$$

(Janesick 2001) where S_D is the total deferred charge (in e^-) in the overscan region, S_{LC} is the charge level in e^- of the last illuminated column or row, and N_P is the number of pixel transfers in the appropriate CCD register. Note that the EPER method does *not* generally provide a reliable measure of CTI proper. First of all, the method measures the amount of charge *deferral* across the whole chip, and is thus only an indirect measure of CTI. Secondly, charge lost or deferred over time scales much longer than the CCD clocking periods is not detected. Thirdly, charge tails that are longer than the width of the overscan region are not accounted for. However, the method does provide a robust *relative* measure of the CTI which can be used to track the time dependence of the CTI.

For the STIS CCD, we measure EPER CTI in the parallel and serial clocking directions using spectral flat fields taken with the G750M grating at central wavelengh 6768 Å. The measurements are done by means of a PyRAF[5] script. The measurement of the parallel EPER CTI involves a slight deviation from Eq. (1) in that the first row of the applicable overscan region suffers from an amplifier "ringing" problem (cf. Goudfrooij & Walsh 1997) which in this case causes a charge much higher than expected for a row in a virtual overscan region. This first overscan row was therefore not considered part of S_D in Eq. (1). The bias level in the parallel overscan region was measured in the regions where the parallel and serial overscans overlap, where no deferred charge can leak into. For the serial EPER CTI measurements, the deferred charge tail is much shorter than the width of the applicable overscan region so that the appropriate bias level can easily be measured from the few columns closest to the edge of the CCD (i.e., the left edge in case of the default readout amplifier 'D').

Derived values for parallel and serial EPER CTI as a function of observation epoch since STIS installation are shown in the left and right panels of Fig. 7, respectively. We draw attention to three points of note regarding Fig. 7:

---

[5]PyRAF is a product of the Space Telescope Science Institute, which is operated by AURA for NASA
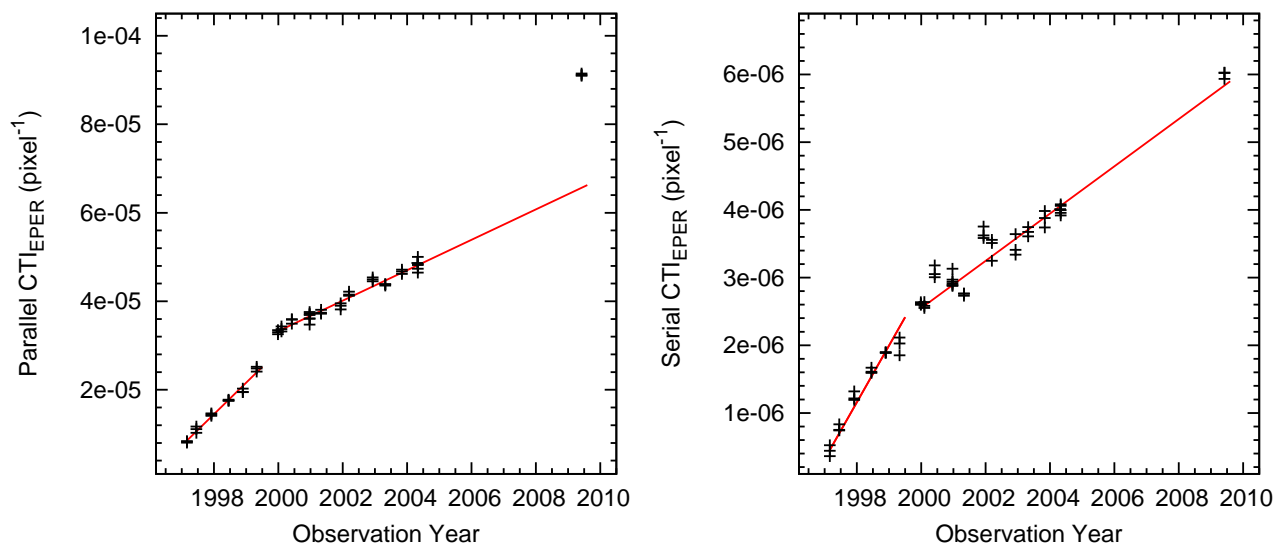
Figure 7: *Left panel:* Parallel EPER CTI vs. time as measured from spectral flat field images with a mean signal level of about 10^4 e$^-$. Error bars are not shown to avoid crowding; the errors are similar to the scatter of points at a given date. *Right panel:* Same as left panel, but for serial EPER CTI. The two red solid lines in both panels indicate linear fits to the pre-2005 data before and after epoch 2000.0 (which is right after SM3a).

1. The EPER CTI measurements are of high accuracy, allowing one to identify clear trends with time, even for the serial CTI whose values are very small (e.g., a typical value of 5×10^{-6} pixel^{-1} yields a charge loss of only 0.25% at the center of the CCD).

2. Also noticeable is a change in the slope of the time dependence of the EPER CTI around epoch 2000.0, which is right after HST Servicing Mission 3a. (Incidentally, this time coincides with a sudden increase in the CCD read noise (cf. Fig. 1))

3. Finally, Fig. 7 shows that the *parallel* EPER CTI values measured in SMOV4 data are *significantly higher than* the extrapolated trend to the $2000-2004$ data, whereas the *serial* EPER CTI values from SMOV4 data are *consistent with* the extrapolated trend. This finding is discussed further below.

A Temperature Dependence of Parallel CTE?

While this significant difference in the behaviors of parallel vs. serial EPER CTI values in SMOV4 data (point 3 mentioned above) seemed strange at face value, we did notice that the SMOV4 EPER data were taken while the CCD housing temperature (header keyword OCCDHTAV, cf. § 3.2 above) was a few degrees higher than in any EPER data taken during side-2 operations before the failure of STIS in Aug 2004. While we do not know quantitatively how changes in the CCD housing temperature relate to changes in the actual CCD temperature, the CCD temperature was probably also higher in the SMOV4 data than in the pre-2004 failure data. To evaluate whether the increase in parallel EPER CTI may indeed be related to CCD temperature, we plot the ratio of the measured CTI values to the CTI values indicated by the time dependence fit (i.e., the red line in the left panel of Fig. 7) versus the CCD housing temperature in Fig. 8. This does show a systematic trend in that higher housing temperatures correspond to higher EPER CTI values. However, the slope of the trend would have to become steeper at OCCDHTAV $> 21\,^{\circ}$C than below if temperature were the dominant reason for the higher parallel CTI values in the SMOV4 data.
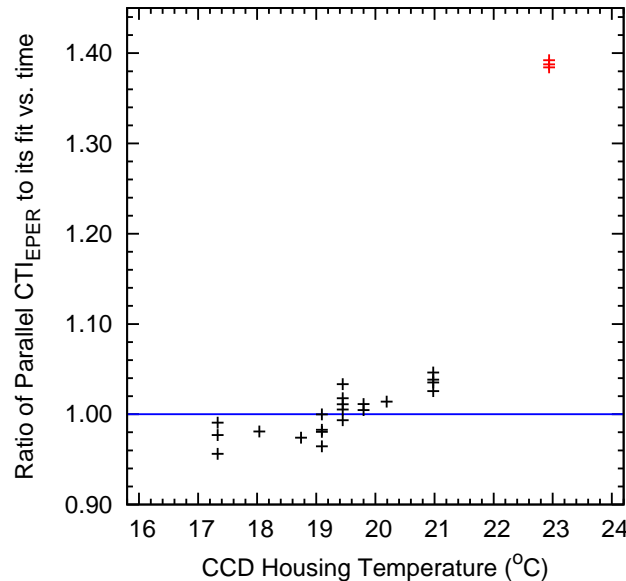
9

Figure 8: Ratio of measured parallel EPER CTI to its time fit (shown in the left panel of Fig. 7) for EPER datasets taken after July 2001 versus CCD housing temperature (header keyword OCCDHTAV; this is used as a proxy to measure changes in CCD temperature since the switch to side-2 electronics in July 2001). The SMOV4 data points are shown in red. Error bars are not shown to avoid crowding; the errors are smaller than the typical scatter of points at a given date. Note the indication of a significant dependence of the parallel CTI on CCD temperature, especially at OCCDHTAV $\gtrsim 21\,°C$.

On the other hand, the operating temperature of the STIS CCD ($\sim -83\,°C$) is actually in the range where the parallel CTI is expected to depend strongly on CCD temperature. Specifically, the "E center" charge trap[6], which is commonly assumed to be a major cause of parallel CTE loss in cooled CCDs with parallel clock periods $\gtrsim 100\,\mu s$ (e.g., Robbins, Roy, & Watts 1991; Holland 1991; Dale et al. 1993), shows a rapid change in CTI in the temperature range -90 to $-60\,°C$, with the exact location of the steepest part of the slope depending on the time between charge packets (i.e., the clocking time). Since the latter is 23.2 ms for the STIS CCD in the parallel clocking direction (Bristow & Alexov 2002), the study of Hardy, Murowinski, & Deen (1998) indicates that the steepest part of the slope is indeed expected near $-80\,°C$ for the STIS CCD. In contrast, the serial clocking speed of the STIS CCD is much faster (22 μs). In that case, the steep increase of CTI is expected to start at a much higher CCD temperature ($\sim -40\,°C$, cf. Hardy et al. 1998), which is consistent with the fact that the serial EPER CTI in the SMOV4 data is compatible with the extrapolated trend derived from the pre-SM4 data.

These expectations from laboratory CCD test data are consistent with the results shown in Figs. 7 and 8. A proper correction of STIS CCD data for CTE loss may therefore, in principle, require a temperature-dependent term in the future, especially if higher CCD housing temperatures (as seen in the EPER data acquired during SMOV4) persist in the coming months. However, one would first have to accumulate enough data at different housing temperatures before being able to derive such a temperature-dependent term at adequate accuracy. The STIS team has implemented appropriate calibration programs to allow such a calibration in the future; this, however, can be expected to take several months.

---

[6]The "E center" trap is a phosphorus-vacancy complex, and hence sometimes called "P–V" trap

5.2   Internal Sparse Field Test

In contrast to the EPER method described above, the "internal sparse field" test for STIS (Kimble, Goudfrooij, & Gilliland 2000) *does* measure "actual" charge loss within a default extraction aperture in spectroscopic mode, and it has been conducted with the STIS CCD on an annual basis in a uniform manner during ground testing as well as in-flight operation of STIS.

A full description of this test is provided in Goudfrooij et al. (2006b,c) and will not be repeated here. Briefly, a sequence of nominally identical exposures is taken, alternating the readout between amplifiers (hereafter amps) located on opposite sides of the CCD. After correcting for (small) gain differences in the two readout amplifier chains, the observed ratio of the fluxes measured by the two amps is fit to a simple CTI model of constant fractional charge loss per pixel transfer (i.e., per row for parallel CTI measurements).

The implementation of this test for the purpose of measuring parallel CTI is as follows. Using the onboard tungsten lamp, the image of a narrow slit which runs along the dipersion direction[7] is projected at five positions along the CCD columns. At each position, a sequence of exposures is taken, alternating between the 'A' and 'C' amps for readout[8]. The calibration program numbers and dates of each observing epoch since STIS was first installed on *HST* are given in Table 1. During SMOV4, exposures were only taken for the default CCDGAIN = 1 setting.

Table 1: Observing blocks of the internal sparse field test for CCDGAIN = 1. Each block extended over a time period of one to a few days. Representative values for the civil date are also shown.

Gain	Block	Program	Date (UT)
1	1	8414	Sep 07, 1999
1	2	8414	Apr 16, 2000
1	3	8851	Oct 28, 2000
1	4	8910	Oct 28, 2001
1	5	9620	Oct 20, 2002
1	6	9620	Sep 14, 2003
1	7	11850	Jul 04, 2009

For each exposure, the average flux per column integrated over a 7-row extraction aperture (which is the default extraction size for long slit STIS spectra of point sources) is calculated. The background level was measured in the same way as the 1-d spectral extraction module of the CALSTIS pipeline. Fluxes and backgrounds were clipped in order to reject residual cosmic rays and hot pixels. The alternating exposure sequence allows one to separate CTI effects from flux variations produced by warmup of the internal tungsten lamp. As the slit image extends across hundreds of columns, high statistical precision on CTI performance can be obtained even at low signal levels per column.

---

[7]Such slits are "special" apertures meant for calibration purposes only; their orientation is perpendicular to the slits used for 'normal' STIS spectra

[8]Before SM4, amps 'B' and 'D' were used for this purpose; amp B was found to exhibit an electronic bit skip ever since SM4, which is why this test now uses amps 'A' and 'C'.

Time Dependence of CTE Degradation

To determine the time dependence of the CTI from this method, all CTI measurements were first normalized to zero background. This involves two steps: First, the effect of the spurious charge in STIS CCD bias frames (cf. § 2.2) was accounted for by considering the total background (B') to be the measured one (B) plus the spurious charge[9]. Second, the previously derived background dependency of the CTI (Goudfrooij et al. 2006b) was taken into account. The time dependence was subsequently determined by fitting the zero-background CTI values (CTI_0) by a function of the form:

$$CTI\,(t) = CTI_0\,[1 + \alpha(t - t_0)], \tag{2}$$

with t in years and $t_0 = 2000.6$, which was the approximate midpoint in time of in-flight STIS observations prior to SM4.

Table 2: CTE degradation time constant α as a function of signal level for gain = 1. The last row lists our newly adopted value in boldface font.

Signal (DN)	α (yr^{-1})	σ_α (yr^{-1})
60	0.221	0.010
130	0.195	0.012
195	0.176	0.018
500	0.200	0.023
3450	0.216	0.005
9850	0.168	0.068
$\alpha = \mathbf{0.216 \pm 0.010}$		

Results for the time-dependence fit for gain = 1 are shown in Fig. 9 and Table 2. The functional fit to the data is quite good, and the derived values for α in Eq. (2) are consistent with one another (within the uncertainties) for all signal levels measured. As to the final selection of the time constant α, we considered that the dataset with 3450 electrons per column is the only one for which pre-flight measurements were available, i.e., it covers a time interval considerably longer than for the other signal levels. Hence $\alpha = 0.216 \pm 0.010$ was selected as representative for all signal levels, as indicated in Table 2. Note that this value for α is consistent with the one used for the full "close-out" calibration of pre-2005 STIS CCD data ($\alpha = 0.218 \pm 0.038$, cf. Goudfrooij et al. 2006b,c).

Finally, the sparse field CTI test data acquired during SMOV4 had "low" CCD housing temperatures (OCCDHTAV values between 16.6 and 18.0 °C), so that the possibility mentioned in § 3.1.1 above (i.e., higher parallel CTI for high CCD temperatures) could not (yet) be tested.

The results mentioned in §§ 2.1, 2.2, 4, and 5.2.1 have been incorporated in a newly delivered CCD reference table (header keyword CCDTAB). STIS CCD data taken after May 11, 2009 and downloaded through the On-The-Fly-Recalibration (OTFR) pipeline after Sep 10, 2009 will have been calibrated with this new table.
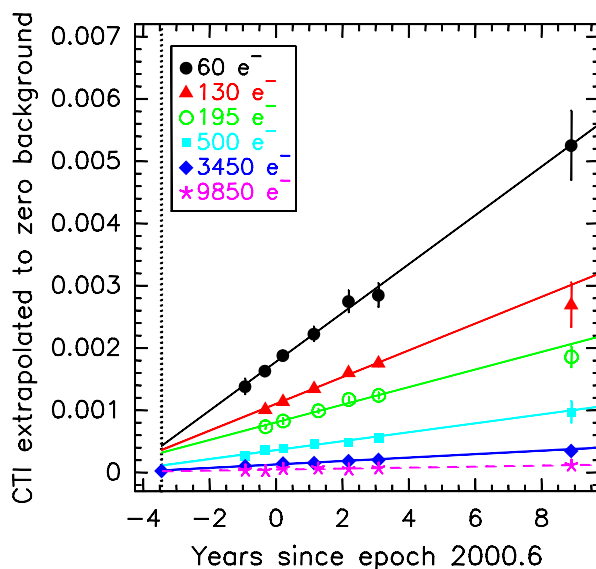
Figure 9: CTI extrapolated to zero background for CCD gain = 1, derived from the internal sparse field test. Both the data and the corresponding linear fits are plotted. The legend shows the signal levels associated with the six symbol types. The dotted vertical line indicates the epoch of HST Servicing Mission 2 (March 1997) during which STIS was installed on HST.

5.3 CTE Correction Formula: Insights from Standard Star Spectra

A good test of the current applicability of the correction formula for CTE loss, as determined before the STIS failure, is provided by STIS CCD spectra of flux standard stars taken during SMOV4[10]. These spectra cover a large range of source count rates along the dispersion, which renders them particularly sensitive to the accuracy of the CTE correction. However, a proper comparison of SMOV4 spectra with older ones should also take into account that the sensitivity of these observing modes is also dependent on time and temperature (Stys, Bohlin & Goudfrooij 2004), and these dependencies have changed somewhat during the long hiatus in STIS operations before its revival in SM4. (The latter dependencies will be presented in detail in § 6 below.) After taking these changes into account, we show comparisons of spectra of the flux standard AGK+81D266 taken in July 2009 vs. in July 1998 (when the CTE loss was still relatively small) in Fig. 10, both in uncorrected net counts and in calibrated fluxes. The combination of the time-dependent sensitivity calibration and the CTE correction is able to calibrate the observed net count ratio of 1.1 to 1.2 to a flat unity in flux space, to within a rms uncertainty of 1.0%. The efficacy of the CTE correction formula is illustrated most clearly in panels (c) and (d) of Fig. 10: The G430L spectra reached rather low source counts at the short-wavelength end, so that the CTE correction factor is relatively large in that region for the 2009 spectrum relative to the 1998 spectrum. However, the CTE correction formula corrects the difference to within the Poisson noise (compare panels (c) with (d) of Fig. 10).

---

[9]The spurious charge values are measured from contemporaneous bias frames taken during the observing blocks listed in Table 1

[10]The correction for CTE loss is part of the on-the-fly-recalibration (OTFR) pipeline CALSTIS
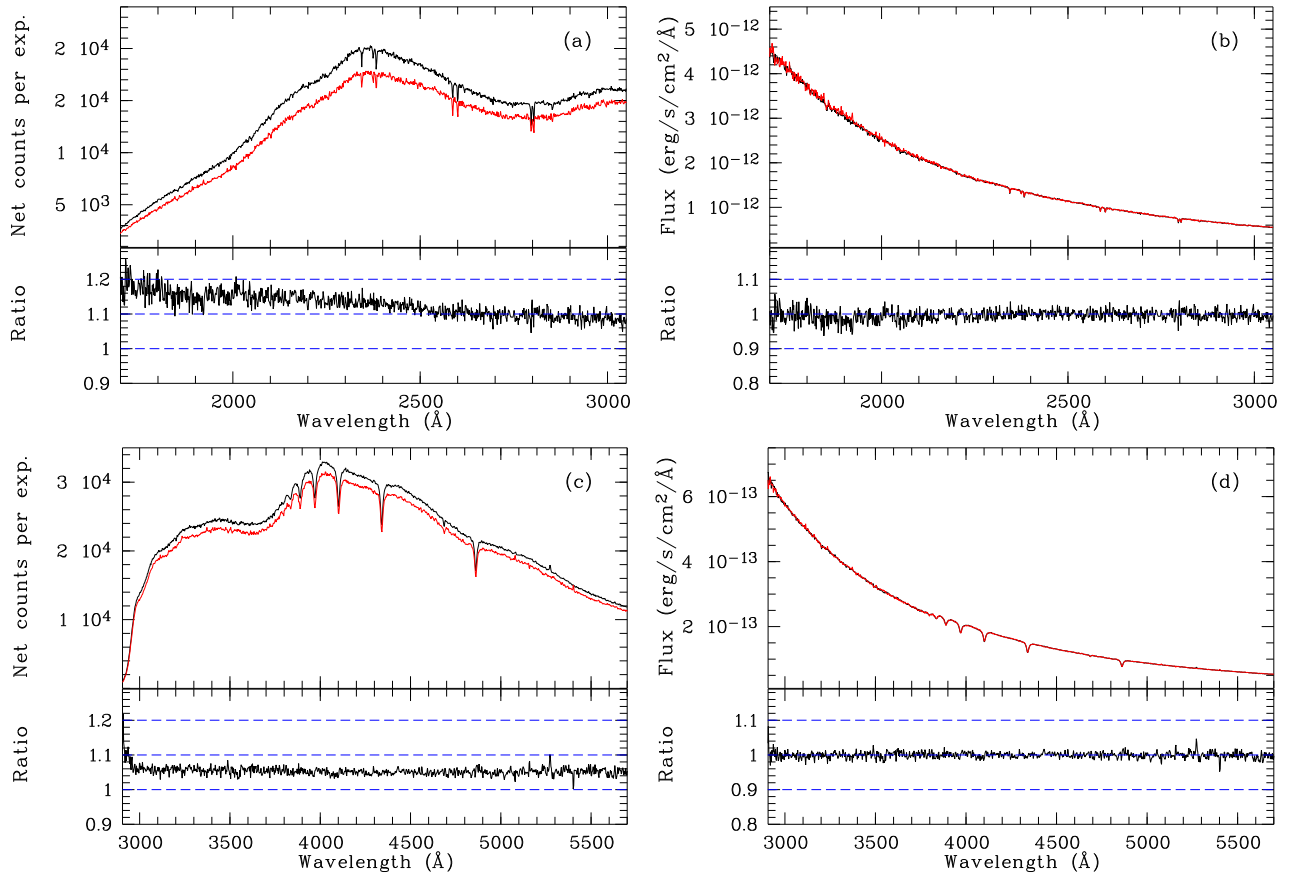
Figure 10: *Panels (a):* The top subpanel shows the net counts in G230LB spectra of flux standard star AGK+81D266 with rootnames o45a13010 (observing date July 1998; in black) and oa9j01050 (July 2009; in red). The bottom subpanel shows the ratio of the two spectra along with horizontal blue dashed lines to guide the eye. *Panels (b):* Same as panels (a), but now showing the calibrated fluxes in F_λ after correction for time-dependent sensitivity and CTE loss using the new calibration reference files. *Panels (c):* Same as panels (a), but now for G430L spectra of flux standard star AGK+81D266 with rootnames o45a12020 (observing date July 1998; in black) and oa9j01080 (July 2009; in red). *Panels (d):* Same as panels (b), but now for the G430L spectra shown in panels (c). See discussion in § 5.3.

6 Spectroscopic Sensitivity: Dependence on Time and Temperature

To detect changes in spectroscopic sensitivity due to (e.g.) cumulative contamination of optics, the subdwarf AGK+81D266 has been monitored on a regular basis for all three CCD low-dispersion gratings, using the $2''$-wide 52x2 slit. These spectra are and have been taken in a uniform manner (in terms of exposure times etc.) ever since 1997 when STIS was first installed on *HST*. Spectroscopic sensitivities are known to change with on-orbit time as well as detector temperature (see Stys et al. 2004 and references therein). The individual dependencies on time and temperature are determined in an iterative manner as follows. After correction for CTE loss according to the prescriptions in Goudfrooij et al. (2006b,c), time dependencies are determined as described in § 6.2 below, and the data are corrected for those time changes. Second, temperature dependencies are determined using the CCD housing temperature as a proxy (for side-2 CCD data only). Data are then

corrected for temperature, after which new time dependencies are calculated. This process is repeated until the next iteration yields results that are within $1\,\sigma$ of the previous one.

6.1 Temperature Dependence of Sensitivity

The correlations between sensitivity and CCD housing temperature are shown in Figs. 11 – 13 for side-2 data after including three AGK+81D266 spectra taken during SMOV4 in each mode. The SMOV4 data yielded extra data points at low as well as high CCD housing temperatures, allowing the determination of more accurate temperature dependencies than those reported by Stys et al. (2004). The newly derived values of the temperature coefficients are compared with the pre-SM4 ones in Table 3 below.

Table 3: Coefficients of Sensitivity Change with CCD Housing Temperature.

Grating	Range	%/°C	
	(Å)	post-SM4	pre-SM4
G230LB	1900 – 2900	$+0.304 \pm 0.018$	$+0.332 \pm 0.019$
G430L	3300 – 5300	$+0.263 \pm 0.032$	$+0.200 \pm 0.050$
G750L	5900 – 8700	$+0.079 \pm 0.022$	$+0.047 \pm 0.022$

Influence of temperature dependence of CTE loss

To evaluate the possibility that the temperature dependencies of the sensitivities determined this way are affected by a temperature dependence of the parallel CTE loss (cf. § 5.1.1 above), we checked for a correlation between the derived slope of the temperature dependence and the mean fraction of CTE loss experienced by the data in the individual wavelength intervals. If the effect of a temperature dependence of the CTE loss is significant, one would expect data with lower-than-average CCD temperature to be "overcorrected" for CTE loss relative to data with higher CCD temperatures. Fig. 14 shows a plot similar to Fig. 11 for the data taken with the G230LB grating[11], where the mean data in each individual wavelength interval in each spectrum is now represented by a data point, and each data point's symbol color indicates the level of its CTE correction factor applied by the CALSTIS pipeline. Linear fits to the data of the different symbol colors do indicate an (albeit small) effect of temperature-dependent CTE loss. However, the amplitude of the effect stays below 1% for all cases measured so far, rendering it negligible for most purposes at this time. Taking into account the possibility that the (housing) temperature of STIS CCD data will rise to higher (average) values in the post-SM4 environment, the STIS team will continue to monitor this effect during Cycle 17 and beyond, and implement corrections to CALSTIS if required.

6.2 Time Dependence of Sensitivity

After correcting the observed net count rates of the CCD modes for CTE loss and temperature, Figs. 15 – 17 show the time dependence of the sensitivity of the three low-dispersion modes after taking into account three post-SM4 datasets. The mean of the net count rates for each observation is divided by the mean of the net count rates for the start time of the first time segment. These relative sensitivities are plotted versus time and

---

[11]The G230LB data were chosen for this purpose because both the temperature dependence and the range of CTE loss values are greater for G230LB data of flux standard stars than for G430L and G750L.
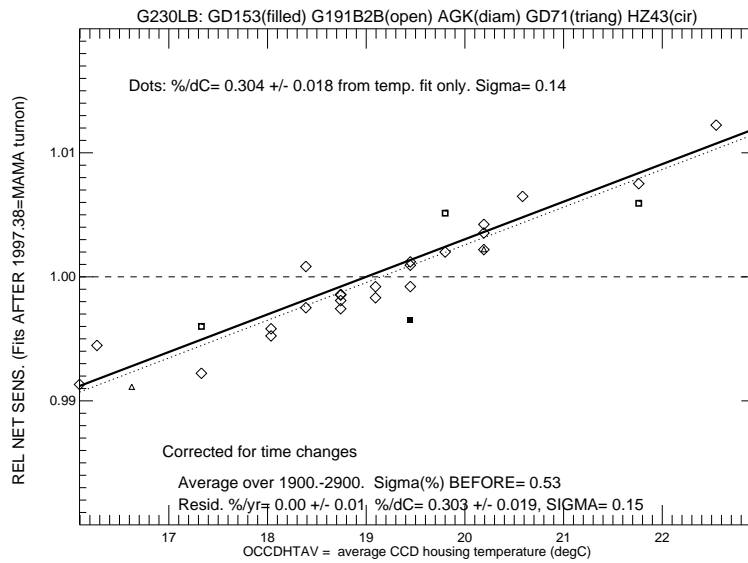
Figure 11: Temperature dependence of sensitivity for G230LB grating. The ordinate represents the ratio of the measured sensitivity to the sensitivity indicated by the pure time dependence fit. Different symbols represent spectra of different standard stars as mentioned in the top label. The solid line represents a linear least-squares fit to the diamonds (i.e., the AGK+81D266 spectra) only.

fitted with linear segments to allow a good fit at any given epoch. The percent-per-year changes in sensitivity and their 1-σ uncertainties for each time segment are printed near the bottom of each panel in Figs. 15 – 17. The inclusion of the post-SM4 sensitivity data caused only very slight changes in the slopes of the (last) time segments of each mode relative to the slopes that were in place before SM4, i.e., there is no evidence of any "special" kind of contamination of the optics occurring after the STIS failure in August 2004.

The newly derived time- and temperature dependencies for spectroscopic CCD data have been incorporated in a new time-dependent sensitivity reference table (header keyword TDSTAB). STIS CCD data taken after May 11, 2009 and downloaded through the OTFR pipeline after Sep 10, 2009 will have been calibrated with this new table. The corresponding table in SYNPHOT (which is used by the HST Exposure Time Calculators) was also updated on Sep 25, 2009. The wavelength-dependent time dependencies derived for the G230LB, G430L, and G750L gratings are also applied to data taken with the G230MB, G430M, and G750M gratings, respectively.

Acknowledgments

References

Bristow, P., & Alexov. A., 2002, ST-ECF Instrument Science Report CE-STIS-2002-001 (Garching: ESA/ST-ECF)

Brown, T. M., 2001, STIS Instrument Science Report 2001-03 (Baltimore: STScI)

Dale, C., Marshall, P., Cummings, B., Shamey, L., & Holland, A. D., 1993, *IEEE Trans. Nucl. Sci.*, Vol. 40, 1628
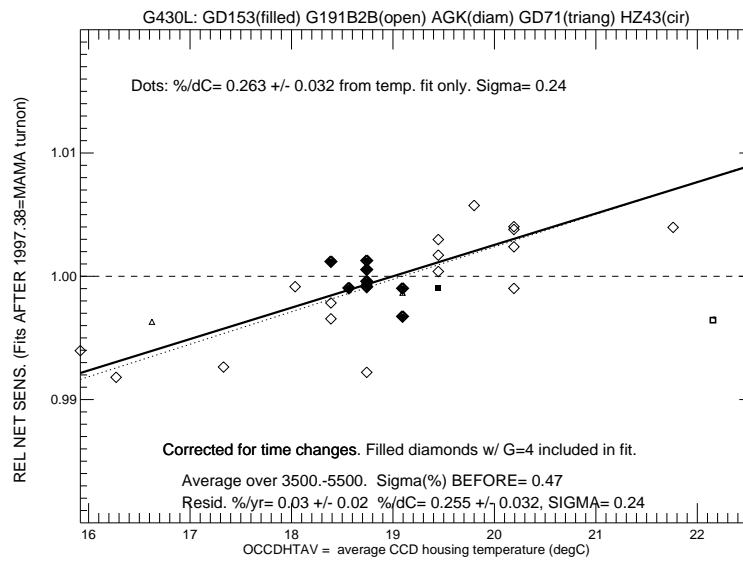
Figure 12: As Fig. 11, but for the G430L grating.

Dashevsky, I.., McGrath, M. A., et al. 2000, STIS Instrument Science Report 2000-04 (Baltimore: STScI)

Diaz-Miller, R. I., Goudfrooij, P., et al. 2001, STIS Instrument Science Report 2001-04 (Baltimore: STScI)

Dressel, L., Davies, J. E., et al. 2004, STIS Instrument Science Report 2004-06 (Baltimore: STScI)

Goudfrooij, P., & Walsh, J. R., 1997, STIS Instrument Science Report 1997-09 (Baltimore: STScI)

Goudfrooij, P., Beck, T., Kimble, R. A., & Christensen, J. A., 1997, STIS Instrument Science Report 1997-10 (Baltimore: STScI)

Goudfrooij, P., & Bohlin, R. C., 2006, STIS Instrument Science Report 2006-03 (Baltimore: STScI)

Goudfrooij, P., et al., 2006a, in Proc. 2005 HST Calibration Workshop, eds. A. M. Koekemoer, P. Goudfrooij, & L. L. Dressel (Baltimore: STScI), p. 181

Goudfrooij, P., Bohlin, R. C., Maíz-Apellániz, J., & Kimble, R. A., 2006b, PASP, 118, 1455

Goudfrooij, P., Maíz-Apellániz, J., Brown, T. M., & Kimble, R. A., 2006c, STIS Instrument Science Report 2006-01 (Baltimore: STScI)

Hardy, T., Murowinski, R., & Deen, M. J. 1998, *IEEE Trans. Nucl. Sci.*, Vol. 45, 154

Holland, A. D., 1991, *Inst. Phys. Conf. Ser.*, 121, 33

Janesick, J. R., 2001, "Scientific Charge-Coupled Devices" (Bellingham: SPIE Press)

Janesick, J. R., Soli, G., Elliot, T., & Collins, S., 1991, "The effects of proton damage on charge-coupled devices", in *Proc. SPIE*, 1447, 87

Hayes, J. J. E., Christensen, J. A., & Goudfrooij, P., 1998, STIS Instrument Science Report 98-06 (Baltimore: STScI)

Kimble, R. A., Goudfrooij, P., & Gilliland, R. L., 2000, Proc. SPIE, 4013, p. 532

Proffitt, C. R., Davies, J. E., et al. 2003, STIS Instrument Science Report 2003-02 (Baltimore: STScI)

Robbins, M. S., Roy, T., & Watts, S. J., 1991, *Proc. RADECS* 91, Vol. 15, 327

Smith, E., Stys, D., Walborn, N., & Bohlin, R. C., 2000, STIS Instrument Science Report 2000-03 (Baltimore: STScI)

Stys, D. J., Bohlin, R. C., & Goudfrooij, P., 2004, STIS Instrument Science Report 2004-04 (Baltimore: STScI)

Wolfe, M. A., Davies, J. E., Proffitt, C. R., Goudfrooij, P., & Diaz, R. I., 2009, STIS Instrument Science Report 2009-01 (Baltimore: STScI)
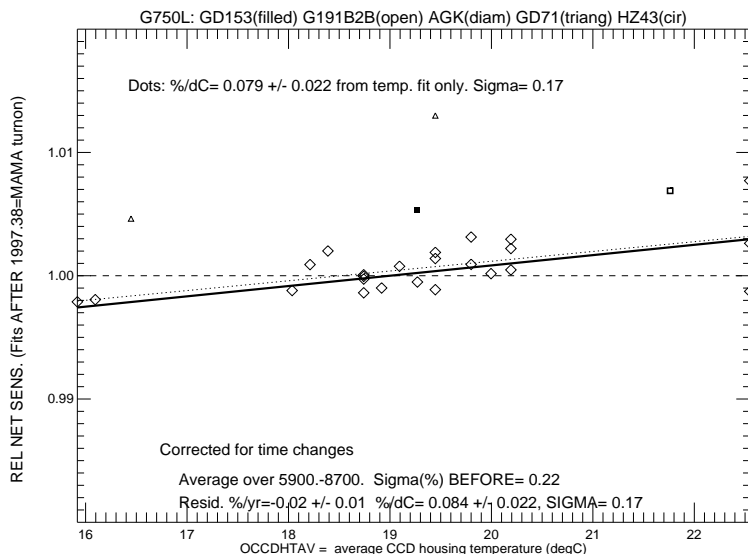
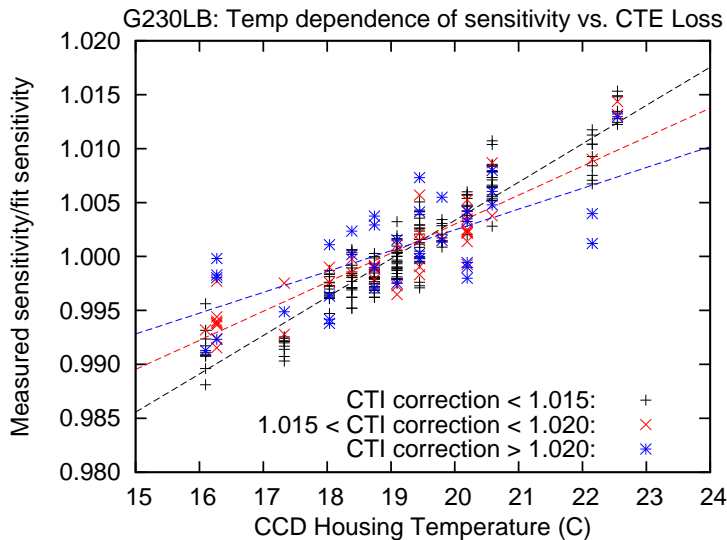**Figure 13**: As Fig. 11, but for the G750L grating.

Figure 14: Similar to Fig. 11, but the mean data in every individual wavelength interval for each G230LB spectrum now has its own symbol. The symbol color indicates the multiplicative factor of the CTE correction applied to the data point in question, as shown in the legend. The three lines represent linear least-square fits to the data points of the corresponding colors. The slope of the fit decreases with increasing correction for CTE loss, indicating a small temperature dependence of the CTE loss. See discussion at the end of § 6.1.
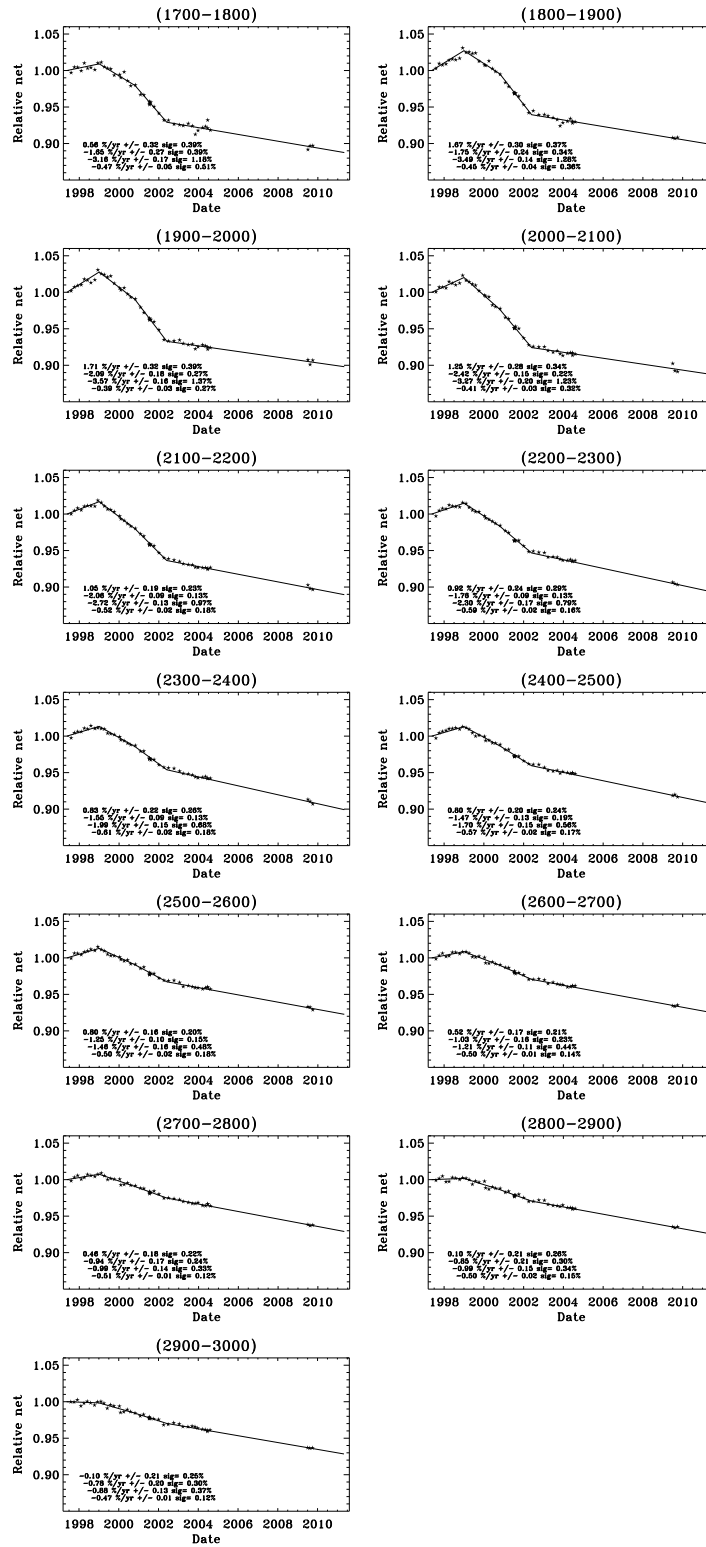
Figure 15: Relative sensitivity versus observing date for G230LB in 100 Å bins (wavelength intervals covered by the bins are indicated at the top of each panel).
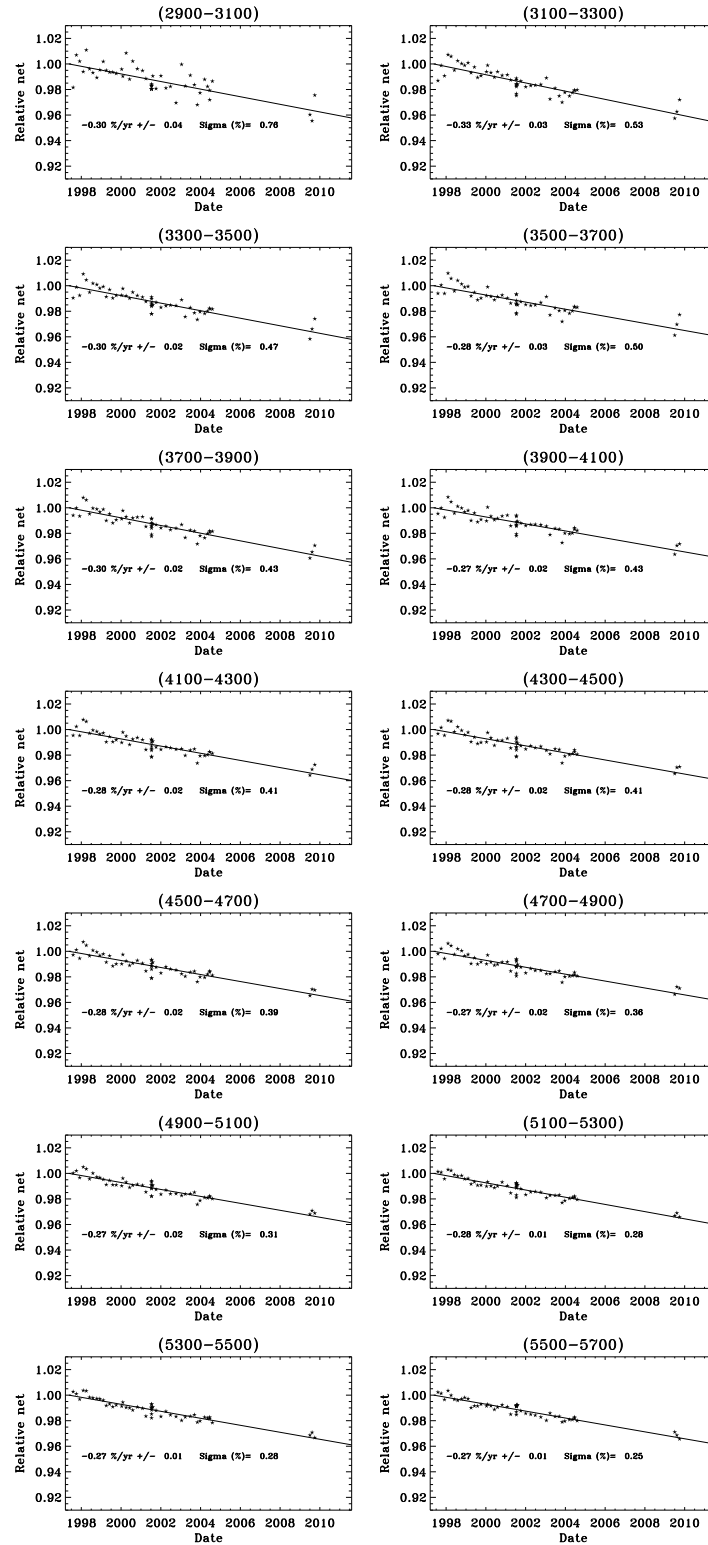
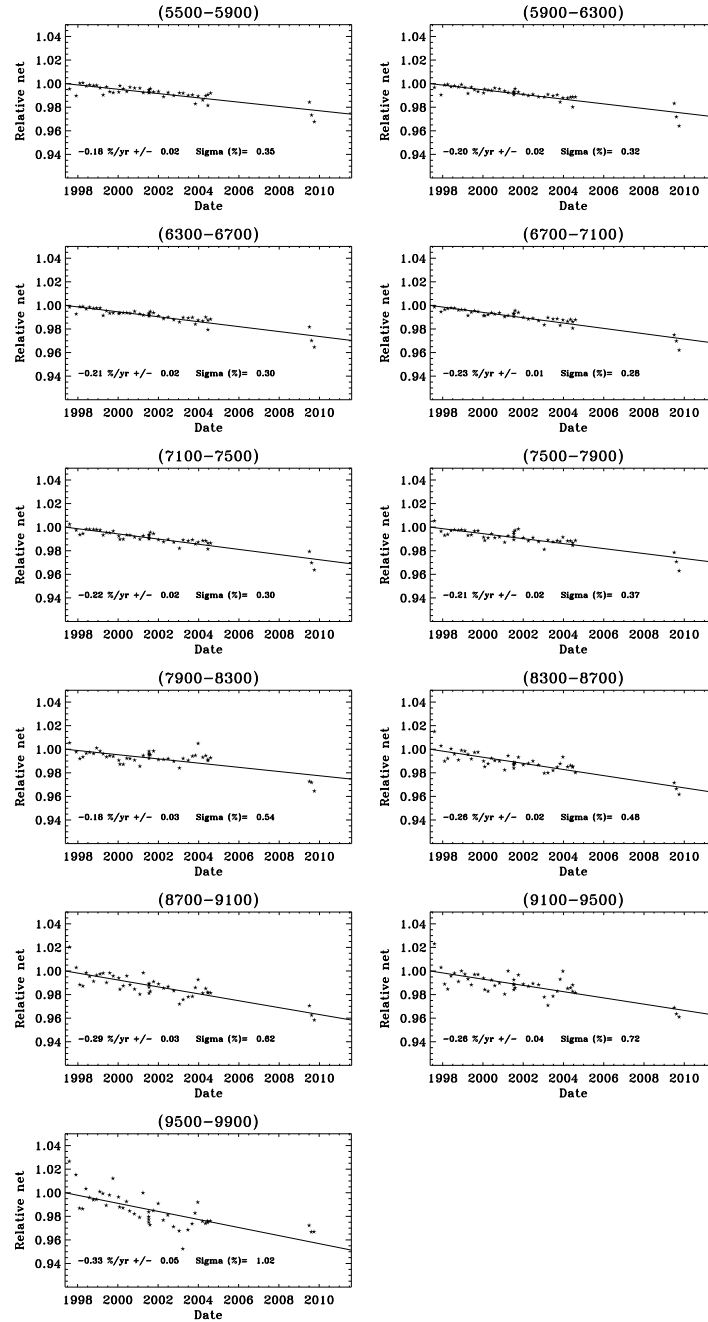**Figure 16**: Relative sensitivity versus observing date for G430L in 200 Å bins.

Figure 17: Relative sensitivity versus observing date for G750L in 400 Å bins.